PAPER

Distinguishing electronic contributions of surface and sub-surface transition metal atoms in Ti-based MXenes

To cite this article: Yizhou Yang et al 2020 2D Mater. 7 025015

View the article online for updates and enhancements.

Recent citations

- <u>Tunable electrochromic behavior of titanium-based MXenes</u> Geetha Valurouthu *et al*
- <u>Pseudocapacitance: From Fundamental</u> <u>Understanding to High Power Energy</u> <u>Storage Materials</u> Simon Fleischmann *et al*
- Computational Screening of 2D Ordered Double Transition-Metal Carbides (MXenes) as Electrocatalysts for Hydrogen Evolution Reaction Di Jin et al

2D Materials



RECEIVED 17 September 2019

17 September 201

20 December 2019

ACCEPTED FOR PUBLICATION

8 January 2020

PUBLISHED 5 February 2020

PAPER

Distinguishing electronic contributions of surface and sub-surface transition metal atoms in Ti-based MXenes

Yizhou Yang¹®, Kanit Hantanasirisakul¹³², Nathan C Frey³®, Babak Anasori¹³²⁴®, Robert J Green⁵³6, Paul C Rogge¹, Iradwikanari Waluyo७, Adrian Hunt७, Padraic Shafer®®, Elke Arenholz®, Vivek B Shenoy³, Yury Gogotsi¹³²® and Steven J May¹®

- ¹ Department of Materials Science and Engineering, Drexel University, Philadelphia, PA 19104, United States of America
- ² A.J. Drexel Nanomaterials Institute, Drexel University, Philadelphia, PA 19104, United States of America
- ³ Department of Materials Science and Engineering, University of Pennsylvania, Philadelphia, PA 19104, United States of America
- Department of Mechanical and Energy Engineering, Integrated Nanosystems Development Institute, Purdue School of Engineering and Technology, Indiana University—Purdue University Indianapolis, Indianapolis, IN 46202, United States of America
- ⁵ Department of Physics and Engineering Physics, University of Saskatchewan, Saskatoon, Saskatchewan S7N 5E2, Canada
- ⁶ Stewart Blusson Quantum Matter Institute, University of British Columbia, Vancouver, British Columbia V6T 1Z4, Canada
- 7 Brookhaven National Laboratory, National Synchrotron Light Source II, Upton, NY 11973, United States of America
- ⁸ Advanced Light Source, Berkeley, Lawrence Berkeley National Laboratory, CA 94720, United States of America
- Ornell High Energy Synchrotron Source, Cornell University, Ithaca, NY 14853, United States of America

E-mail: smay@drexel.edu

Keywords: MXene, x-ray absorption spectroscopy, electronic structure, titanium

Supplementary material for this article is available online

Abstract

MXenes are a rapidly-expanding family of 2D transition metal carbides and nitrides that have attracted attention due to their excellent performance in applications ranging from energy storage to electromagnetic interference shielding. Numerous other electronic and magnetic properties have been computationally predicted, but not yet realized due to the experimental difficulty in obtaining uniform surface terminations (T_x) , necessitating new design approaches for MXenes that are independent of surface terminations. In this study, we distinguished the contributions of surface and sub-surface Ti atoms to the electronic structure of four Ti-containing MXenes (Ti₂CT_x) $Ti_3C_2T_x$, $Cr_2TiC_2T_x$, and $Mo_2TiC_2T_x$) using soft x-ray absorption spectroscopy. For MXenes with no Ti atoms on the surface transition metal layers, such as $Mo_2TiC_2T_x$ and $Cr_2TiC_2T_x$, our results show minimal changes in the spectral features between the parent MAX phase and its MXene. In contrast, for MXenes with surface Ti atoms, here $Ti_3C_2T_x$ and Ti_2CT_x , the Ti L-edge spectra are significantly modified compared to their parent MAX phase compounds. First principles calculations provide similar trends in the partial density of states derived from surface and sub-surface Ti atoms, corroborating the spectroscopic measurements. These results reveal that electronic states derived from sub-surface M-site layers are largely unperturbed by the surface terminations, indicating a relatively short length scale over which the T_x terminations alter the nominal electron count associated with Ti atoms and suggesting that desired band features should be hosted by sub-surface M-sites that are electronically more robust than their surface M-site counterparts.

1. Introduction

The large family of 2D materials known as MXenes [1–4] has attracted intense interest due to their suitability for solution processing, hydrophilic surfaces, metallic conduction, and versatility in hosting a range of intercalant ions and molecules leading to excellent performance in applications including electrodes for supercapacitors and batteries

[5–9], electromagnetic interference shielding [10–14], and flexible antennas [15, 16]. The general chemical formula for MXenes is $M_{n+1}X_nT_x$, where M is an early transition metal, X is carbon or nitrogen, and T_x represents surface species such as =O, –OH, and –F. MXenes can consist of multiple elements on the M-site, either as random alloys or in ordered arrangements [17–19]. Synthesis of solid solution MXenes such as $(Ti_{0.5},Nb_{0.5})_2C$ and $(V_{0.5},Cr_{0.5})_2C$ with randomly-

mixed transition metals on the M-site was reported in 2012 [20]. More recently, ordered double-M MXenes (M'₂M"C₂T_x or M'₂M"C₃T_x) were realized following the discovery of ordered Cr₂TiAlC₂ MAX phase, in which the Cr and Ti atoms occupy separate planes along the *c*-axis [21]. The expansion of MXenes into ordered double-M chemistries not only broadens the array of compositions that can be accessed but also provides two distinct M-sites—surface and subsurface positions—that may contribute differently to the functional properties.

The electronic properties of MXenes have been explored mainly through temperature-dependent resistivity measurements, spectroscopic methods, and density functional theory (DFT) calculations [1,2,4,17, 22–29]. Much of this work has highlighted the effects of surface terminations and intercalation on the macroscopic electronic behavior. Depending on processing conditions and post-synthesis annealing procedures, the ensemble resistivity (ρ) of the same nominal MXene compound film (stack of several 2D MXene flakes) can vary by orders of magnitude and $d\rho/dT$ can be either positive or negative. For example, transport measurements are often dominated by interflake hopping that is sensitive to interlayer spacing, intercalated molecules, and surface-bound terminations as a result of the processing to convert MAX phases to MXenes [27, 30–32]. Moreover, instead of providing detailed unoccupied state information, resistivity only provides a narrow view of overall electronic structure near the Fermi level. Electron-based spectroscopies reveal that the electronic band structure of Ti₃C₂T_x is modified during annealing in vacuum due to desorption of surface species. DFT has been used to predict many properties of MXenes including magnetic ordering, semiconductor band gaps, and the presence of topological band features in MXenes [18, 33–49]. However, these predictions strongly depend on the specific T_x terminations used in the calculations, which due to practical limitations of DFT, such as the supercell size, are commonly performed with uniform surface terminations. However, MXenes are known to host complex, spatially inhomogeneous, and synthesis-dependent surface chemistries [50, 51].

While this previous body of work has demonstrated that surface T_x terminations alter the electronic properties of MXenes, the extent to which these terminations modify the electronic behavior of all M-site-derived bands or just the surface-most M-site atoms is currently unknown. Clearly, a detailed and layer-resolved understanding of the impact of T_x terminations is critically important for interpreting how and why the experimental properties of MXenes deviate from computational predictions. However, this issue has not yet been experimentally explored, largely owing to the difficulty in separating electronic contributions arising from distinct M-site layers within MXenes. For instance, resistivity experiments only provide information on the ensemble behaviour of

all layers, with intrinsic electronic behavior often obscured by interflake hopping processes. However, newly realized ordered double-M MXenes provide a unique opportunity to tailor the location of Ti within the material, from solely occupying the surface layers in ${\rm Ti}_2{\rm CT}_x$ to residing in the sub-surface layers in ${\rm Mo}_2{\rm Ti}_2{\rm C}_2{\rm T}_x$, thus allowing for the interactions of the ${\rm T}_x$ terminations with Ti layers to be systematically tuned. By applying an elementally-resolved probe of electronic structure to a systematically-selected set of Ti-containing MXenes, we provide a direct measure of the differing electronic contributions of surface and sub-surface Ti atoms in MXenes.

In this study, we take advantage of the elemental specificity offered by x-ray absorption spectroscopy (XAS) to measure the unoccupied electronic states derived from Ti atoms in Ti_2CT_x , $Ti_3C_2T_x$, $Mo_2TiC_2T_x$, and $Cr_2TiC_2T_x$ MXenes in comparison with their corresponding Al-containing MAX phases. We show that in Ti_2CT_{∞} which has all Ti atoms located on its surface, the Ti $L_{2,3}$ -edge spectra exhibit significant changes upon conversion from Ti₂AlC MAX to the Ti₂CT_x MXene. In contrast, MXenes with only sub-surface Ti atoms (Mo₂TiC₂T_x and Cr₂TiC₂T_x) exhibit minimal spectral changes following transformation from their parent MAX phases (Mo₂TiAlC₂ and Cr₂TiAlC₂, respectively), which we attribute to decreased interaction strength between surface terminations and the sub-surface transition metal. Additionally, we show the robustness of the sub-surface M-site contributions to the electronic structure through DFT calculations that reveal the T_x influence on Ti-derived bands is significantly decreased in Mo₂TiC₂T_x (no surface Ti atoms) compared to Ti_2CT_x and $Ti_3C_2T_x$ (with surface Ti atoms). This work points to the importance of deriving desired electronic and magnetic function from sub-surface M-site layers, laying out an important design principle in the ongoing search for robust magnetic or topological behavior in MXenes.

2. Methods

2.1. Sample preparation

Ti₂AlC MAX phase was synthesized following a protocol reported previously [20]. Ti_2CT_x was produced by etching 2g of the MAX powder in a mixture of LiF (3g, Alfa Aesar) and 9 M HCl (20 ml, Fisher) at 35 °C for 15h. The mixture was washed with DI water in two 175 ml tubes and centrifuged at 3500 rpm for 5 min. The washing process was repeated 3–4 times until a dark supernatant was obtained. The dark supernatant was decanted and the sediment was transferred to a 50 ml tube and hand-shaken vigorously for 10 min. Finally, the mixture was centrifuged at 3500 rpm for 1 h and the supernatant was filtered over a porous membrane (3501 Coated PP, Celgard, USA). A free-standing film of Ti₂CT_x was removed from the membrane right after all the solution passed through the membrane. The film was further dried in a vacuum

desiccator and stored in an Ar-filled glovebox to avoid long exposure of the film to ambient air and resultant oxidation.

To synthesize Ti₃C₂T_x, 2g of Ti₃AlC₂ (Materials Research Center, Ukraine) was etched in a premixed solution LiF (3g, Alfa Aesar) and 9 M HCl (20 ml, Fisher) at 35 °C for 24h. The washing protocol was similar to that of Ti₂CT_x. The final supernatant was filtered over a porous membrane (3501 Coated PP, Celgard, USA). The film was dried on the filtration setup overnight and further dried in a vacuum desiccator.

Mo₂TiAlC₂ MAX phase was synthesized following a protocol reported elsewhere [17]. Mo, Ti, Al and graphite powders (all from Alfa Aesar, Ward Hill, MA) with a molar ratio of 2:1:1.1:2 were ball-milled for 18 h using zirconia balls in plastic jars. The powder mixtures were heated in covered alumina crucibles at 5 °C min⁻¹ to 1600 °C and held for 4h under argon. After cooling, the porous compacts were milled and sieved through a 400 mesh sieve, producing powders with a particle size $<38 \mu m$. To synthesize Mo₂TiC₂T_x, 2 g of the MAX powder was added to 40 ml of 48%-51% aqueous HF solution and stirred at 50 °C for 48 h. The mixture was washed with DI water in two 175 ml tubes for at least 5 times or until the pH of the supernatant was higher than 5. Then the powder was collected over a PVDF membrane (5 μ m, Millipore). To delaminate $Mo_2TiC_2T_x$ powder, 1 g of the powder was stirred in 10 ml of tetrabutylammonium hydroxide (TBAOH) aqueous solution (48 wt%, Sigma Aldrich) for 12h. The mixture was washed with DI water and centrifuged at 3500 rpm for 15 min. The washing process was repeated 3 times. After a pH of 7-8 was reached, the supernatant was decanted and the sediment was dispersed in 30 ml of DI water and bath-sonicated (2510, Branson) at 40 kHz for 30 min in a water-ice sonication bath under argon bubbling. The final solution was centrifuged at 3500 rpm for 30 min and the supernatant was filtered the same way as Ti_2CT_x .

Cr₂TiAlC₂ MAX phase was synthesized in our laboratory. To synthesize Cr₂TiC₂T_x, 2 g of the MAX powder was added to a pre-mixed etchant containing 50% HF, 12 M HCl, and DI water with a ratio of 2:3:5. The mixture was stirred at 35 °C for 42 h and washed in a similar way to Mo₂TiC₂T_x. To delaminate Cr₂TiC₂T_x, 2 g of the etched mixture was stirred in 20 ml of TBAOH (25% in water, Aldrich). The mixture was washed with DI water and centrifuged at 3500 rpm for 15 min. The washing process was repeated 3–4 times. After a pH of 7–8 was reached, the supernatant was decanted and the sediment was dispersed in 25 ml of DI water and probe-sonicated (Fisher Scientific model 505 Sonic Dismembrator) for 30 min in a water-ice sonication bath under argon bubbling.

The phase purity and compositions of all MXenes was verified by x-ray diffraction (XRD) and x-ray photoelectron spectroscopy (XPS) as shown in figures S1 and S2 (stacks.iop.org/TDM/7/025015/mmedia) in the supporting information. XRD results show the

002 peaks of MXene phases are at lower 2θ position relative to their corresponding MAX phases, which indicates an expansion of the the c-axis parameter. The Al 2p region in the photoemission spectra obtained from each MXene suggest the Al atoms in the MAX phases are fully etched away, except that there is a negligible amount of Al left in the $Cr_2TiC_2T_x$ MXene after etching.

2.2. XAS measurement

 $L_{2,3}$ -edge XAS measurements were performed at National Synchrotron Light Source II (NSLS-II) beamline 23-ID-2 (IOS) and the Advanced Light Source (ALS) beamline 4.0.2. The Ti L-edge was measured between 450 eV to 480 eV with an energy step size of 0.05 eV. The spectra used in this study were collected in total electron yield mode. All XAS measurements were performed at room temperature and under ultra-high vacuum.

2.3. DFT Calculations

DFT calculations were performed using the Vienna ab initio simulation package (VASP) [52]. The Perdew-Burke-Ernzerhof (PBE) [53] exchange-correlation functional and projector augmented wave (PAW) pseudopotentials [54] were used for all calculations. Structural relaxations were performed with a 520 eV plane-wave basis cutoff and a 10 \times 10 \times 1 Γ centered k-point mesh until forces on each atom were converged to below 10^{-2} eV Å⁻¹. Total energies were converged to 10^{-8} eV and a dense $21 \times 21 \times 1 \Gamma$ centered k-point mesh was used for computing densities of states. Calculations for $Cr_2TiC_2T_x$ were performed with and without spin polarization and a Hubbard U parameter of 4 eV for Cr, following previous DFT predictions of magnetic ordering in functionalized Cr₂TiC₂. MXenes [18, 55]. The Ti d-orbital-derived projected density of states (PDOS) was not significantly affected with spin polarization, so non-spin polarized results are reported here.

3. Result and discussion

In order to investigate the effects of the Ti site occupancy within the MXene layers, three types of MXenes were investigated: compounds with (i) Ti atoms only on the surface (Ti_2CT_x) , (ii) Ti atoms in both the surface and the middle transition metal layer $(Ti_3C_2T_x)$, and (iii) Ti atoms residing in only the center M-site layer ($Mo_2TiC_2T_x$ and $Cr_2TiC_2T_x$). Schematics of these structures, along with their corresponding Al-containing parent MAX phases [56], are shown in figure 1. When the Al layer is etched out from Ti₂AlC (figure 1(a)), both layers of Ti in Ti_2CT_x are exposed to the surface terminations. Figure 1(b) shows that when the Al layer is selectively etched from Ti₃AlC₂, the remaining MXene contains three layers of Ti, the top and bottom surface layers are similar to the Ti layers in Ti₂CT_x, while the center Ti layer is not bonded to

 IOP Publishing
 2D Mater. 7 (2020) 025015
 Y Yang et al

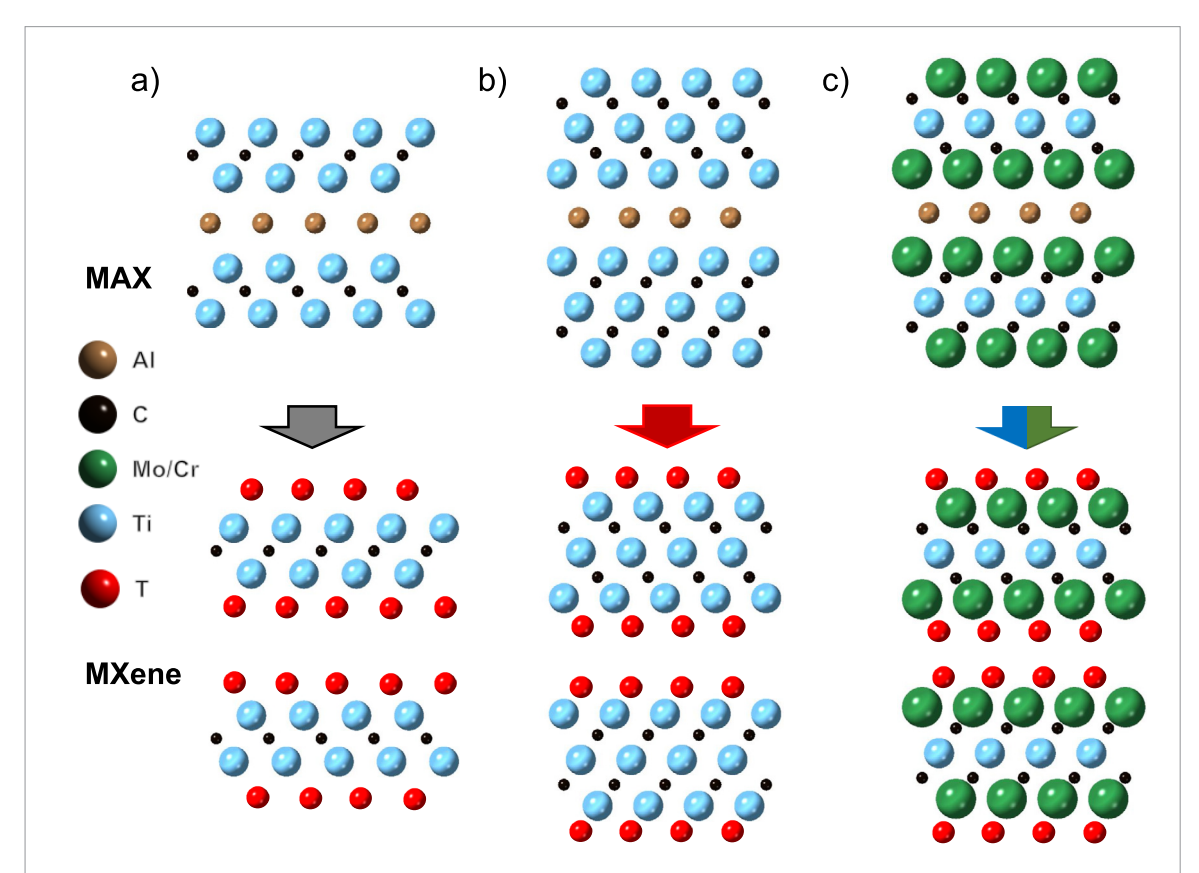


Figure 1. Schematic of MAX phases (top) and MXenes (bottom) investigated in this study. The MXenes are synthesized by removal of the Al layer in the MAX structures via selective chemical etching, a process that leaves behind a variety of surface terminations (T_x) on the surface transition metal layers. (a) The conversion of Ti_2AlC to Ti_2CT_x MXene where all Ti atoms reside on surface sites, while (b) $Ti_3C_2T_x$ hosts both surface and sub-surface Ti atoms, and (c) $Mo_2TiC_2T_x$ and $Cr_2TiC_2T_x$ exhibit ordered M-site arrangements, in which the Ti atoms reside in the middle transition metal layer (sub-surface Ti). The T_x atoms (red) represent the mixed surface terminations (O^{2-} , F^- , OH^-) that are covering the surface transition metals.

the surface terminations. In contrast, when the Al layer is etched away from Mo₂TiAlC₂ and Cr₂TiAlC₂ (figure 1(c)), the only Ti layer in the resulting MXenes is sandwiched by two MoC or CrC layers in the subsurface M-sites and does not directly bond to the surface terminations. Therefore, comparison of these four compounds allows us to directly probe the role of surface and sub-surface Ti atoms on the electronic structure. Here we note that the M-layers in ordered double-M MXenes are nominally fully ordered [17, 57], although studies quantifying the degree of ordering are currently limited.

In figure 2, we present the Ti $L_{2,3}$ -edge spectra for all MAX and MXene studied here. The spectral features arise from electronic transitions in which electrons are excited from the occupied Ti 2p core-level orbitals to unoccupied Ti 3d valence orbitals. The spectra contain both the L_3 (~453–463 eV) and L_2 (~463–473 eV) edges, which are a result of spin–orbit splitting of the p-orbitals producing distinct $2p_{1/2} \rightarrow 3d$ (L_2) and $2p_{3/2} \rightarrow 3d$ (L_3) transitions. The measured spectra are thus reflective of the unoccupied Ti 3d density of states, but do not map directly onto the DOS due to interactions with the core hole created upon excitation. The MXene spectra shown in figure 2 are representative of spectra obtained from multiple samples at different locations on the samples.

Data over the wider spectral range from 450 eV to 480 eV are presented in figure S3 in the supporting information. All the spectra shown in this study were normalized by subtracting the average pre-edge intensity (450-455 eV) from the raw spectra, and then by scaling the entire spectrum so that the postedge absorption at 471 eV is set to unity. This postedge energy was chosen to avoid the presence of single-hump-features between 473 eV to 480 eV which adversely affects the normalization process. The sample homogeneity and stability under x-ray flux was examined by measuring multiple positions on each of the samples. The x-ray absorption spectra are almost identical for the same sample at different positions as shown in figure S4, indicating homogeneity of the samples. Also, each spot was measured twice resulting in unchanged spectra, which suggests that the samples do not degrade with exposure to the soft x-ray beam during the time of spectra collection (~15 min). Different batches of MXene samples were measured twice at NSLS-II and once at ALS. For all the MXene samples, the spectra are consistent across the three measurements, as shown in figure S5, confirming the reproducibility of the MXene spectra.

Significant modifications to the spectral shapes are observed in Ti₂CT_x and Ti₃C₂T_x with respect to their parent Ti₂AlC and Ti₃AlC₂ MAX phases. Single-M

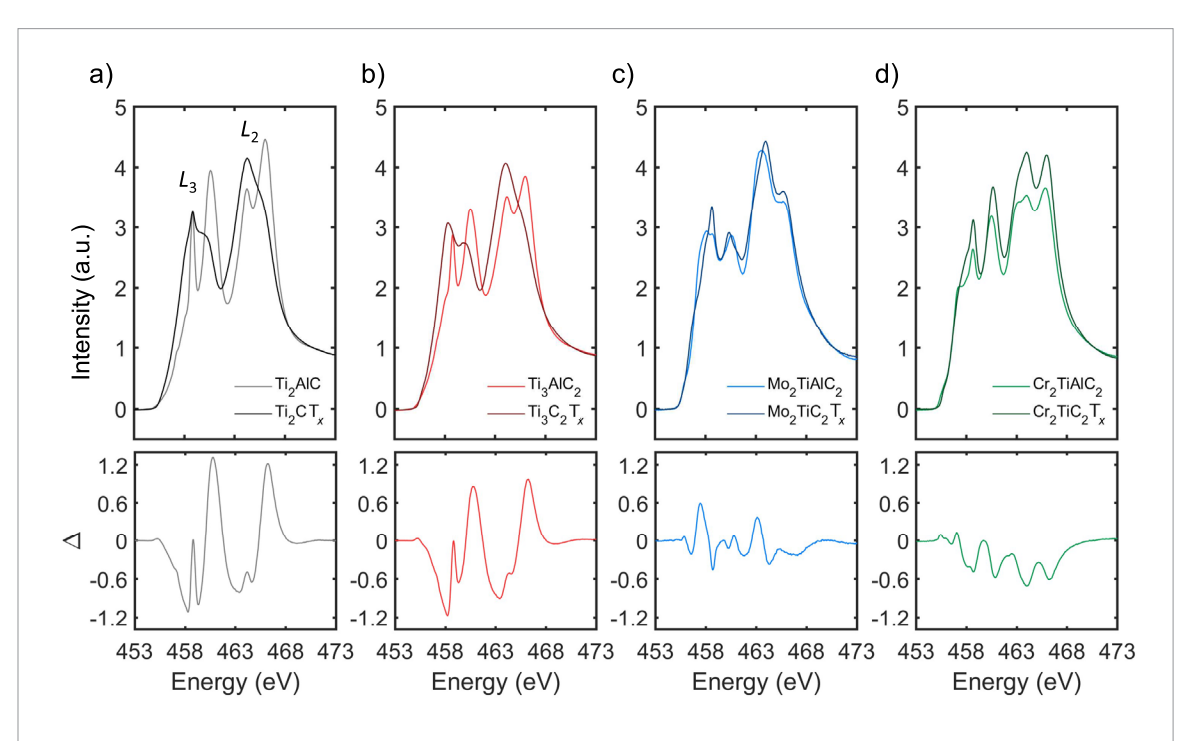


Figure 2. X-ray absorption spectra measured from (a) Ti_2CT_x and Ti_2AlC_x (b) $Ti_3C_2T_x$ and Ti_3AlC_x (c) $Mo_2TiC_2T_x$ and Mo_2TiAlC_x , and (d) $Cr_2TiC_2T_x$ and Cr_2TiAlC_x at the TiL_x -edge. In all data sets, MXene spectra are represented by the darker lines and the MAX spectra are represented by the lighter lines. Bottom panels display difference spectra (Δ) obtained by subtracting each MXene spectrum from its parent MAX phase spectrum.

MXene spectra (figures 2(a) and (b)) have two noticeable changes from their parent MAX. First, the MXene spectral features are broadened with respect to the parent MAX phases. Second, the absorption peaks are shifted to lower energy in the MXene phase. In contrast, the spectra from the ordered double-M MXenes (figures 2(c) and (d)) are very similar to that of their parent MAX phases. To further illustrate the Ti *L*-edge evolution from MAX to MXene, we present the difference spectra (Δ) as defined by subtracting the MXene spectra from the MAX spectra shown in the bottom panels of figure 2. As all x-ray absorption spectra were normalized by the same process, the magnitude of the features in Δ can be directly compared between samples in order to quantify the relative spectral changes. Ti_2CT_x has the largest differences among all the samples, with features in the Δ spectrum approximately two times larger than that of the double-M MXenes.

We note that the difference spectra of Ti_2CT_x and $Ti_3C_2T_x$ show similar features (figures 2(a) and (b)). When the Al layers are etched away, the bonding of the surface metal layer changes, from M-Al to M-T bonds. To further verify that the sub-surface metal layer (the center Ti layer here) is spectrally distinct from the surface metal atoms, we subtracted the Ti_2CT_x spectrum (containing only Ti surface atoms) multiplied by 2/3 from the $Ti_3C_2T_x$ spectrum (containing both surface and sub-surface Ti atoms), and the result is shown in figure S6 in the supporting information. Unlike the Ti_2CT_x and $Ti_3C_2T_xL_3$ -edge region, which has a broad peak with a shoulder feature, the difference spectrum shown in figure S6 has a clear splitting in the L_3 -edge. This L_3 splitting is also observed in the ordered

double-M MXene spectra, suggesting that after eliminating the contribution from the surface transition metals through this spectrum subtraction process, the center Ti layer in $\text{Ti}_3\text{C}_2\text{T}_x$ is electronically similar to the Ti-derived bands in $\text{Cr}_2\text{Ti}\text{C}_2\text{T}_x$ and $\text{Mo}_2\text{Ti}\text{C}_2\text{T}_x$. This implies that the interactions between the center Ti layer in $\text{M}_3\text{C}_2\text{T}_x$ and the surface terminations are minimal compared to the M-T_x interactions in M_2CT_x MXene.

To further quantify the degree of changes to the electronic structure upon conversion from MAX to MXene, we calculated the integral of Δ^2 ($\int_{E_{pre-edge}}^{E_{pre-edge}} \Delta^2 dE$) from the pre-edge to post-edge energy for each difference spectra as shown in figure 3(a). Ti₂CT_x has the largest integrated Δ^2 among the MXenes studied here, while the ordered double-M MXenes, in which the majority of Ti atoms reside in the sub-surface layers, have the smallest integrated Δ^2 . This indicates that the spectral changes are more significant for the surface-derived bands than those derived from sub-surface metal atoms, and thus that the T_x terminations have a minimal impact on the subsurface M-atoms compared to the surface M-atoms.

The relative concentration of d-electrons per Ti atoms can be inferred from the branching ratio which is defined as $\frac{\int I[L_3]}{\int (I[L_3]+I[L_2])}dE$, where I is the XAS intensity. Generally, in early transition metals, such as Ti, the branching ratio decreases as the d-orbital occupation decreases [58–61]. For example, in titanium oxides, the branching ratio decreases from 0.505 to 0.451 to 0.372 as electron count is decreased from d^2 to d^1 to d^0 , as further discussed in the supporting information. To

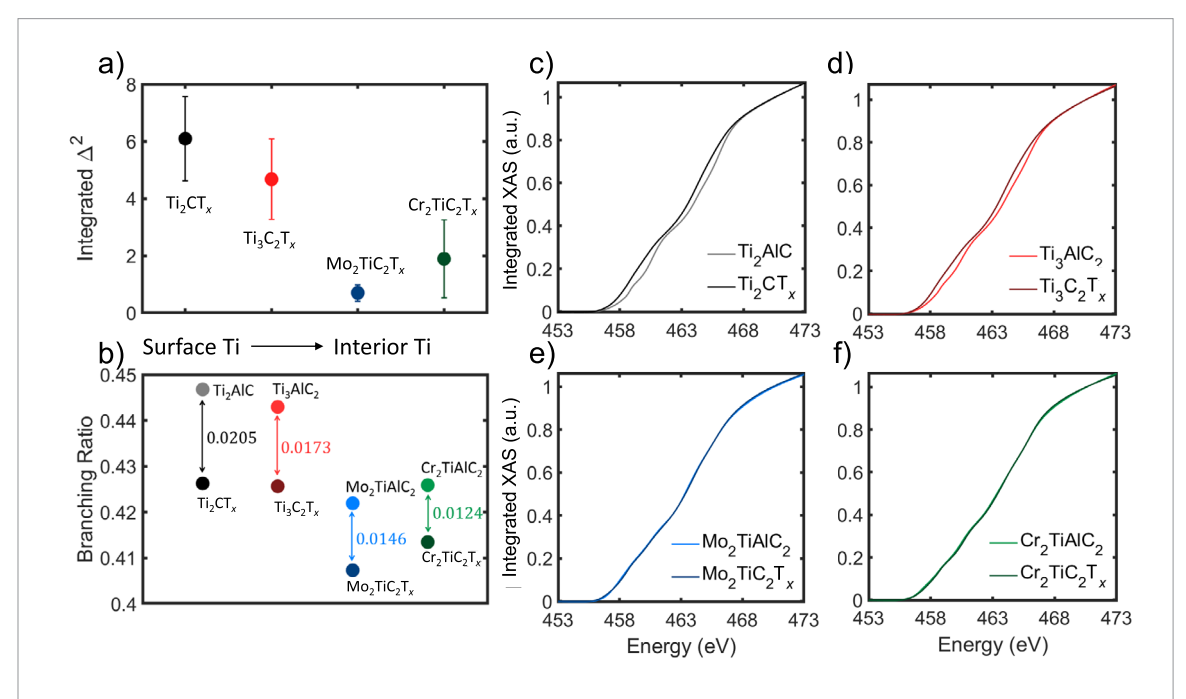


Figure 3. (a) Integrated Δ^2 (difference squared) provides a direct measurement of the differences between MAX and MXene spectra. Error bars are generated by systemically altering the 471 eV post-edge normalization position by ± 2 eV. (b) The branching ratio obtained from each spectrum. Panels (c)–(f) show the normalized integral of the x-ray absorption spectra for MXene and MAX compounds from pre-edge (455 eV) to post-edge (471 eV). Significant shifts in the leading absorption edge are only observed in the MXenes containing surface Ti.

obtain accurate integrals within the L_2 and L_3 regions, an edge jump background was subtracted from the spectra prior to the branching ratio calculation based on Pearson et al's normalization method [62]. Figure 3(b) shows the differences in branching ratio between MAX and the corresponding MXenes. In all cases, the branching ratio decreases upon conversion of MAX to MXenes, indicating a decrease in the Ti electron count in MXenes compared to the parent MAX phases. Importantly, the decrease in branching ratio is the largest for MXenes with Ti on the surface sites and is the smallest in ordered double-M MXenes. This result is consistent with DFT calculations that routinely show a decrease in d-electron count in T_xterminated MXenes compared to bare MXenes [23]. Additionally, previous XPS results on Ti₃AlC₂ and $Ti_3C_2T_x$ were interpreted in terms of a decreased electron count in the MXene relative to the corresponding MAX [63].

Next, we consider the integrated XAS spectra as shown in figures 3(c)–(f). The spectra from MXenes that contain surface Ti atoms $(\text{Ti}_2\text{CT}_x$ and $\text{Ti}_3\text{C}_2\text{T}_x)$ exhibit a clear shift to lower energies after conversion from the MAX phases, while that of the MXenes with only sub-surface Ti atoms $(\text{Mo}_2\text{Ti}\text{C}_2\text{T}_x)$ and $\text{Cr}_2\text{Ti}\text{C}_2\text{T}_x)$ do not (figures 3(e)–(f)). These integrals are normalized to the total integrated spectral area up to the post-edge normalization energy $(471\,\text{eV})$. In order to quantify the shift, we calculated the energy shift at every 10% of the normalized spectra integral. The average shift is $-0.53\pm0.16\,\text{eV}$ for Ti_2CT_x , $-0.47\pm0.14\,\text{eV}$ for $\text{Ti}_3\text{C}_2\text{T}_x$, $0.02\pm0.05\,\text{eV}$ for $\text{Mo}_2\text{Ti}\text{C}_2\text{T}_x$, and $-0.03\pm0.04\,\text{eV}$ for $\text{Cr}_2\text{Ti}\text{C}_2\text{T}_x$; the

error bars are calculated from the standard deviation of the shifts and do not take into account instrumental limitations. This shift to lower energies in Ti_2CT_x and $Ti_3C_2T_x$ can be seen in the difference spectra (figures 2(a) and (b)) as the negative Δ feature at the onset of the L_3 absorption edge.

While a shift to lower energies in ionic compounds typically indicates reduction (an increased electron count of the cation), this interpretation is inconsistent with the branching ratio results. We note that the bonds in MXenes are highly covalent and thus an ionic interpretation of XAS based on isolated polyhedral units is likely inappropriate for metallic MXenes with delocalized electrons. Instead, we attribute the spectral shift to changes in the energetic positions of unoccupied Ti bands upon conversion from MAX to MXene, and not to reduction of Ti.

We computed elementally-resolved densities of states with DFT for relevant MXene and MAX compounds to better understand the origin of these spectral shifts. In figure 4, we present the Ti d-orbital-derived PDOS above the Fermi level (E_F) for three types of MAX phases (Ti₂AlC, Ti₃AlC₂, and Cr₂TiAlC₂) and the corresponding O- and F-terminated MXenes. While OH-termination is also commonly observed in MXenes, the transition metal PDOS is not significantly different than that for isoelectronic F-termination [64–67], so we do not consider OH-termination here. We focus on the Ti-derived PDOS above E_F in these compounds as this is the region of the electronic structure probed by XAS.

MXenes with Ti layers on the surface (figures 4(a) and (b)) displayed significant differences in

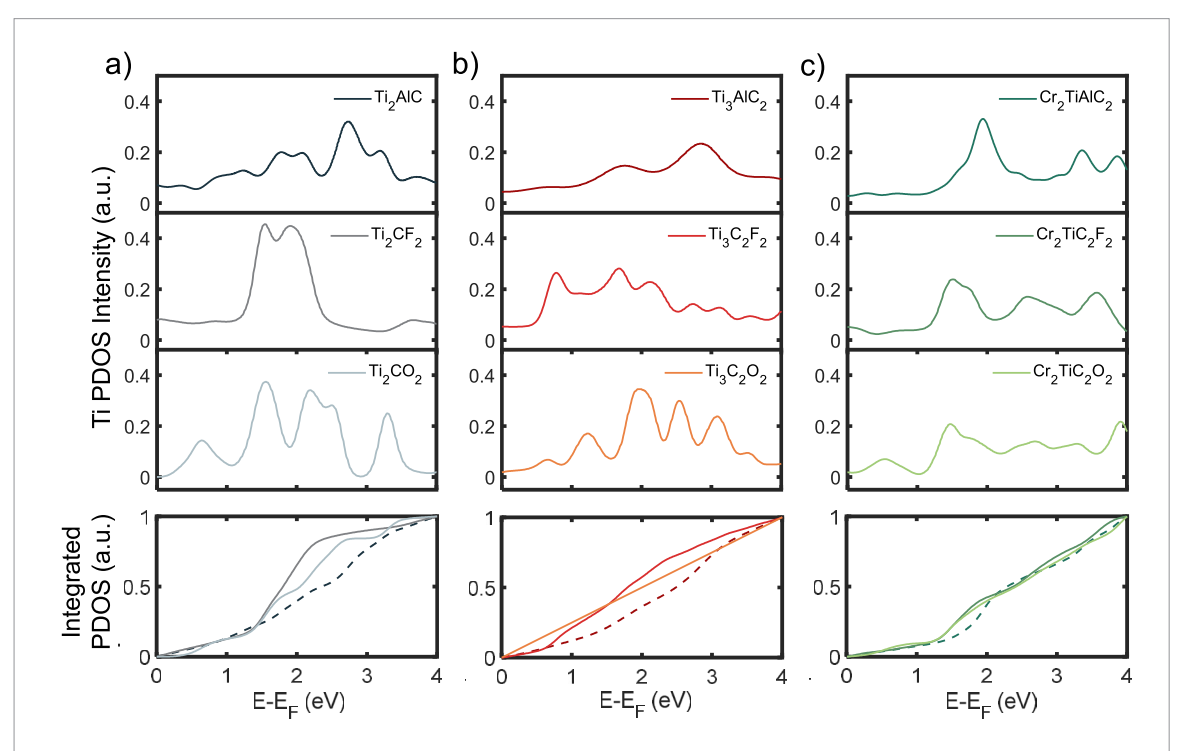


Figure 4. Ti d-orbital-derived unoccupied PDOS calculated for three MAX phases and the corresponding MXenes with Ti at different locations, (a) Ti on the surface in Ti₂AlC and Ti₂CT $_{\infty}$ (b) Ti on both surface and sub-surface sites in Ti₃AlC $_2$ and Ti₃C $_2$ T $_{\infty}$ and (c) Ti at the sub-surface positions in Cr $_2$ TiAlC $_2$ and Cr $_2$ TiC $_2$ T $_{\infty}$. Top panels are parent MAX phases, the second panels are MXenes with pure F termination, and the third panels are MXenes with pure O termination. The bottom panels show the normalized integral of PDOS for MAX (dashed line) and MXene compounds with pure F and O terminations.

the unoccupied electronic structure compared to the corresponding MAX phase, with the Ti PDOS of MXenes systematically shifted to lower energies. The middle two panels of figure 4 display the calculated PDOS for the O- and F-terminated MXenes, revealing the emergence of new peaks in the PDOS and the shifting of states to lower energies as compared to the parent MAX compounds. The shifts to lower energy found for Ti₃C₂T_x and Ti₂CT_x, which are readily visible in the normalized integration of PDOS shown in the bottom panels of figures 4(a) and (b), are qualitatively similar to the spectral shifts measured by XAS (figures 3(c)–(d)). In contrast, the integrated PDOS for Cr₂TiAlC₂ and Cr₂TiC₂T_x display a similar energydependence (figure 4(c)) indicating that the electronic states of sub-surface Ti atoms in $Cr_2TiC_2T_x$ are largely unaffected by surface termination. Similar results were seen in Mo_2TiAlC_2 and $Mo_2TiC_2T_x$ (figure S7).

Using Bader charge analysis, we obtained the change in the Ti atom charge between the MAX and MXene phases and confirm the proposed origin of the spectral shift. In Ti₂AlC, the average electron count is $2.8 \text{ e}^-/\text{Ti}$, while in the Ti₂CT_x MXenes, the average number of 3d electrons per Ti is 2.3– $2.4 \text{ e}^-/\text{Ti}$ for O- and F-terminations. Similarly, for the surface Ti atoms in Ti₃C₂, the Bader charge changes from $2.8 \text{ e}^-/\text{Ti}$ (MAX) to $2.35 \text{ e}^-/\text{Ti}$ (MXene). These changes suggest that the spectral shift can be attributed to changes in the positions of unoccupied Ti bands, rather than a reduction of Ti. However, the Bader charge on the subsurface Ti atoms remains between 2.5– $2.6 \text{ e}^-/\text{Ti}$ for

all MAX and MXene phases considered here, regardless of surface termination or composition. Bader charge values for all transition metals can be found in figure S8. These results support our interpretation of the changes to branching ratio and the origin of the absorption edge shifts upon conversion of MAX to MXene. Furthermore, the stability of the sub-surface Ti charge state and electronic states show the promise of engineering robust electronic, magnetic, and topological features in MXenes without control of the surface chemistry.

4. Conclusions

In summary, we have studied the contribution of Ti atoms residing at surface and sub-surface M-site positions to the electronic structure of MXenes through XAS measurements and DFT calculations of MAX and MXene phases. Mo₂TiC₂T_x and Cr₂TiC₂T_x, MXenes that contain only sub-surface Ti atoms, do not exhibit significant changes in the Ti L-edge spectra after conversion from the corresponding MAX phases. In contrast, Ti_2CT_x and $Ti_3C_2T_x$ exhibit noteable spectral modifications due to the presence of T_x terminations that interact with the surface Ti layers, consistent with previous reports of surface terminations reducing the *d*-band electron count in these materials. The disparate electronic effects of Tx terminations on surface and sub-surface M-sites is further confirmed through DFT calculations of unoccupied PDOS and Ti 3d electron densities. These results indicate that the electronic

Y Yang et al

implications of the T_x terminations are largely accommodated within the surface-most M-site layers and have much more limited impact on sub-surface M-site atoms. With these new insights, we propose a general design strategy to stabilize surface invariant properties in ordered double-M MXenes, wherein the sub-surface M-site atoms are selected to host the desired electronic, magnetic, and topological functionalities.

Acknowledgments

All experimental aspects of this work were supported by the U.S. Department of Energy (DOE), Office of Science, Office of Basic Energy Sciences, grant #DE-SC0018618. This research used resources of beamline 23-ID-2 (IOS) of the National Synchrotron Light Source II, a U.S. Department of Energy (DOE) Office of Science User Facility operated for the DOE Office of Science by Brookhaven National Laboratory under Contract No. DE-SC0012704. VBS acknowledges support by contract W911NF-16-1-0447 from the Army Research Office and also by grants EFMA-542879 and CMMI-1727717 from the U.S. National Science Foundation. NCF was supported by the Department of Defense (DoD) through the National Defense Science & Engineering Graduate Fellowship (NDSEG) Program. This research used resources of the Advanced Light Source, which is a DOE Office of Science User Facility under contract no. DE-AC02-05CH11231. Dr David Pinto is acknowledged for help with synthesis of $Mo_2TiC_2T_x$ samples. Drexel University Core Facilities is acknowledged for providing access to XRD and XPS instruments.

ORCID iDs

Yizhou Yang https://orcid.org/0000-0002-7419-291X

Nathan C Frey https://orcid.org/0000-0001-5291-6131

Babak Anasori https://orcid.org/0000-0002-1955-253X

Padraic Shafer https://orcid.org/0000-0001-9363-2557

Yury Gogotsi https://orcid.org/0000-0001-9423-4032

Steven J May • https://orcid.org/0000-0002-8097-1549

References

- [1] Naguib M, Kurtoglu M, Presser V, Lu J, Niu J, Heon M, Hultman L, Gogotsi Y and Barsoum M W 2011 *Adv. Mater.* 23 4248–53
- [2] Naguib M, Mochalin V N, Barsoum M W and Gogotsi Y 2014 Adv. Mater. 26 992–1005
- [3] Peng J H, Chen X Z, Ong W J, Zhao X J and Li N 2019 *Chem*
- [4] Khazaei M, Mishra A, Venkataramanan N S, Singh A K and Yunoki S 2019 *Curr. Opin. Solid State Mater. Sci.* 23 164–78

- [5] Boota M, Anasori B, Voigt C, Zhao M Q, Barsoum M W and Gogotsi Y 2016 Adv. Mater. 28 1517–22
- [6] Naguib M, Come J, Dyatkin B, Presser V, Taberna P-L, Simon P, Barsoum M W and Gogotsi Y 2012 Electrochim. Commun. 1661–4
- [7] Wen Y, Rufford T E, Chen X, Li N, Lyu M, Dai L and Wang L 2017 Nano Energy 38 368–76
- [8] Come J, Naguib M, Rozier P, Barsoum M W, Gogotsi Y, Taberna P-L, Morcrette M and Simon P 2012 J. Electrochem. Soc. 159 A1368–73
- [9] Anasori B, Lukatskaya M R and Gogotsi Y 2017 Nat. Rev. Mater. 2 1–17
- [10] Shahzad F, Alhabeb M, Hatter C B, Anasori B, Man Hong S, Koo C M and Gogotsi Y 2016 *Science* 353 1137–40
- [11] Feng W, Luo H, Wang Y, Zeng S, Deng L, Zhou X, Zhang H and Peng S 2018 RSCAdv. 8 2398–403
- [12] Han M, Yin X, Wu H, Hou Z, Song C, Li X, Zhang L and Cheng L 2016 ACS Appl. Mater. Interfaces 8 21011–9
- [13] Liu J, Zhang H B, Sun R, Liu Y, Liu Z, Zhou A and Yu Z Z 2017 Adv. Mater. 29 1702367
- [14] Cao M-S, Cai Y-Z, He P, Shu J-C, Cao W-Q and Yuan J 2019 Chem. Eng. J. 359 1265–302
- [15] Choi G et al 2018 Adv. Opt. Mater. 6 1701076
- [16] Sarycheva A, Polemi A, Liu Y, Dandekar K, Anasori B and Gogotsi Y 2018 Sci. Adv. 4 eaau0920
- [17] Anasori B, Xie Y, Beidaghi M, Lu J, Hosler B C, Hultman L, Kent P R C, Gogotsi Y and Barsoum M W 2015 ACS Nano 9 9507
- [18] Sun W, Xie Y and Kent P R C 2018 Nanoscale 10 11962-8
- [19] Tao Q et al 2017 Nat. Commun. 8 14949
- [20] Naguib M, Mashtalir O, Carle J, Presser V, Lu J, Hultman L, Gogotsi Y and Barsoum M W 2012 ACS Nano 6 1322–31
- [21] Liu Z, Zheng L, Sun L, Qian Y, Wang J and Li M 2014 *J. Am. Ceram. Soc.* **97** 67–9
- [22] Anasori B, Shi C, Moon E J, Xie Y, Voigt C A, Kent P R, May S J, Billinge S J, Barsoum M W and Gogotsi Y 2016 Nanoscale Horiz. 1 227–34
- [23] Khazaei M, Ranjbar A, Arai M, Sasaki T and Yunoki S 2017 J. Mater. Chem. C 5 2488–503
- [24] Hantanasirisakul K and Gogotsi Y 2018 Adv. Mater. 30 e1804779
- [25] Zhan C, Naguib M, Lukatskaya M, Kent P R C, Gogotsi Y and Jiang D E 2018 J. Phys. Chem. Lett. 9 1223–8
- [26] Zhang N, Hong Y, Yazdanparast S and Zaeem M A 2018 2D Mater. 5 045004
- [27] Hart J L, Hantanasirisakul K, Lang A C, Anasori B, Pinto D, Pivak Y, van Omme J T, May S J, Gogotsi Y and Taheri M L 2019 Nat. Commun. 10 522
- [28] Yang Y, Umrao S, Lai S and Lee S 2017 J. Phys. Chem. Lett. 8 859–65
- [29] Lai S, Jeon J, Jang S K, Xu J, Choi Y J, Park J-H, Hwang E and Lee S 2015 Nanoscale 7 19390–6
- [30] Wang Z, Kim H and Alshareef H N 2018 Adv. Mater. 30 1706656
- [31] Hantanasirisakul K $\it et\,al\,2019$ Chem. Mater. ${\bf 31}\,2941{-}51$
- [32] Halim J, Moon E J, Eklund P, Rosen J, Barsoum M W and Ouisse T 2018 *Phys. Rev.* B **98** 104202
- [33] Khazaei M, Ranjbar A, Arai M and Yunoki S 2016 *Phys. Rev.* B **94** 125152
- [34] Liang Y, Khazaei M, Ranjbar A, Arai M, Yunoki S, Kawazoe Y, Weng H and Fang Z 2017 *Phys. Rev.* B **96** 195414
- [35] Weng H, Ranjbar A, Liang Y, Song Z, Khazaei M, Yunoki S, Arai M, Kawazoe Y, Fang Z and Dai X 2015 Phys. Rev. B 92 075436
- [36] Si C, Jin K H, Zhou J, Sun Z and Liu F 2016 Nano Lett. 16 6584–91
- [37] Balci E, Akkuş Ü Ö and Berber S 2018 Appl. Phys. Lett. 113 083107
- [38] Balci E, Akkus U O and Berber S 2018 J. Phys.: Condens. Matter
- [39] Zhang X, Zhao X, Wu D, Jing Y and Zhou Z 2015 Nanoscale 7 16020–5

2D Mater. 7 (2020) 025015 Y Yang et al

[40] Dong L, Kumar H, Anasori B, Gogotsi Y and Shenoy V B 2017 J. Phys. Chem. Lett. 8 422–8

- [41] Tan T L, Jin H M, Sullivan M B, Anasori B and Gogotsi Y 2017 ACS Nano 11 4407–18
- [42] Frey N C, Kumar H, Anasori B, Gogotsi Y and Shenoy V B 2018 ACS Nano 12 6319–25
- [43] Yue Y 2017 J. Magn. Magn. Mater. 434 164-8
- [44] Guo J, Legum B, Anasori B, Wang K, Lelyukh P, Gogotsi Y and Randall C A 2018 Adv. Mater. 30 e1801846
- [45] Sternik M and Wdowik U D 2018 Phys. Chem. Chem. Phys. 20 7754–63
- [46] Yang J, Luo X, Zhou X, Zhang S, Liu J, Xie Y, Lv L and Chen L 2017 Comput. Mater. Sci. 139 313–9
- [47] Zhang Y, Xia W, Wu Y and Zhang P 2019 Nanoscale 11 3993– 4000
- [48] Guo Z, Zhou J, Zhu L and Sun Z 2016 J. Mater. Chem. A 4 11446–52
- [49] Si C, Zhou J and Sun Z 2015 ACS Appl. Mater. Interfaces 7 17510–5
- [50] Halim J, Cook K M, Naguib M, Eklund P, Gogotsi Y, Rosen J and Barsoum M W 2016 Appl. Surf. Sci. 362 406–17
- [51] Wang H W, Naguib M, Page K, Wesolowski D J and Gogotsi Y 2016 Chem. Mater. 28 349–59
- [52] Kresse G and Furthmüller J 1996 Phys. Rev. B 54 11169–86
- [53] Perdew J P, Burke K and Ernzerhof M 1996 Phys. Rev. Lett. 77 3865–8
- [54] Kresse G and Joubert D 1999 *Phys. Rev.* B **59** 1758–75

- [55] Yang J, Zhou X, Luo X, Zhang S and Chen L 2016 Appl. Phys. Lett. 109 203109
- [56] Sokol M, Natu V, Kota S and Barsoum M W 2019 Trends Chem. 1 210–23
- [57] Liu Z et al 2014 Acta Mater. 73 186-93
- [58] Crocombette J P and Jollet F 1994 J. Phys. Condens. Matter. 6 10811–21
- [59] Wang Z L, Yin J S, Mo W D and Zhang Z J 1997 J. Phys. Chem. B 101 6793–8
- [60] Varela M, Oxley M, Luo W, Tao J, Watanabe M, Lupini A R, Pantelides S and Pennycook S 2009 Phys. Rev. B 79 085117
- [61] Yedra L, Xuriguera E, Estrader M, Lopez-Ortega A, Baro M D, Nogues J, Roldan M, Varela M, Estrade S and Peiro F 2014 Microsc. Microanal. 20 698–705
- [62] Pearson D H, Ahn C C and Fultz B 1993 *Phys. Rev. B: Condens. Matter* 47 8471–8
- [63] Halim J, Lukatskaya M R, Cook K M, Lu J, Smith C R, Näslund L Å, May S J, Hultman L, Gogotsi Y and Eklund P 2016 Chem. Mater. 26 2374–81
- [64] Schultz T, Frey N C, Hantanasirisakul K, Park S, May S J, Shenoy V B, Gogotsi Y and Koch N 2019 Chem. Mater. 31 6590–7
- [65] Xie Y and Kent P R C 2013 Phys. Rev. B 87 235441
- [66] Berdiyorov GR 2016 AIP Adv. 6 055105
- [67] Bai Y, Zhou K, Srikanth N, Pang J H L, He X and Wang R 2016 RSC Adv. 6 35731–9